Journal of Applied Physics

Quantum-spin-Hall phases and 2D topological insulating states in atomically thin layers

Cite as: J. Appl. Phys. **129**, 090902 (2021); https://doi.org/10.1063/5.0029326
Submitted: 11 September 2020 . Accepted: 16 February 2021 . Published Online: 05 March 2021

Junji Haruyama

AIP Publishing

Journal of Applied Physics PERSPECTIVE scitation.org/journal/jap

Quantum-spin-Hall phases and 2D topological insulating states in atomically thin layers

Cite as: J. Appl. Phys. **129**, 090902 (2021); doi: 10.1063/5.0029326
Submitted: 11 September 2020 · Accepted: 16 February 2021 ·
Published Online: 5 March 2021

Junji Haruyama[1,2,a)]

AFFILIATIONS

[1]Faculty of Science and Engineering, Aoyama Gakuin University, 5-10-1 Fuchinobe, Sagamihara, Kanagawa 252-5258, Japan
[2]Institute for Industrial Science, The University of Tokyo, 4-6-1 Komaba Meguro-ku, Tokyo 153-8505, Japan

Note: This paper is part of the Special Topic on 2D Quantum Materials: Magnetism and Superconductivity.
[a)]**Author to whom correspondence should be addressed:** J-haru@ee.aoyama.ac.jp

ABSTRACT

The quantum-spin-Hall (QSH) phase and its helical edge spins of two-dimensional (2D) topological insulators (TIs) are attracting increasing attention. The helical edge spin currents are a favorite to applications in dissipationless spintronic devices with low error rates because the spin currents existing along sample 1D edges are topologically protected in time-reversal symmetry and are easily controlled by external bias voltages. Moreover, combining the 1D edge spin currents with ferromagnetic or superconductor electrodes yields various exciting phenomena and those applications to innovative quantum devices. Nevertheless, reports of 2D TIs and QSH phases (particularly at high temperatures) have been rare and mainly in semiconductor 2D quantum wells. Here, I introduce and discuss how 2D TI states and QSH phases can be created and applied to innovative quantum (spintronic) devices, particularly in atomically thin layers (such as graphene and transition metal dichalcogenide family, which is energetically studied and have demonstrated large topological bulk gaps recently). Research of 2D TIs on atom-thin (or few) layers and those application must open a door to next-generation quantum architectures (such as topological quantum computation utilizing the Majorana fermion).

I. INTRODUCTION

Research of novel two-dimensional (2D) materials and quantum phenomena observed in them is attracting significant interest. In particular, various quantum phenomena, which arise from those specified spin alignments, are highly interesting, such as 2D magnetism, superconductivity, and spintronic phenomena. Recently, numerous novel quantum phenomena have been observed in atomically thin 2D layers, such as graphene and transition metal dichalcogenide (TMDC) family.

Among those, helical edge spins in the quantum-spin-Hall (QSH) phase of 2D topological insulators (TIs) are highly important. A 2D TI is characterized by a bulk bandgap Δ arising from spin–orbit coupling (SOC) and helical edge spin states along the sample 1D edges within the closed Δ. In the helical edge spin states, opposite-spin electrons form a Kramers doublet and counter-propagate under the protection of time-reversal symmetry (Fig. 1). Consequently, the edge conductance is quantized leading to the QSH phase, which is much different from the conventional quantum Hall effect that originates from just the electron orbital quantization and Landau levels formed under strong magnetic fields. The helical edge spins are suitable for applications to spintronic devices because the 1D spin current path along the sample edges can be easily controlled by external bias voltages with avoiding influence of any geometrical scattering factors.

Nevertheless, reports of 2D TIs have been rare. The main stream has been semiconductor quantum wells. The first experimental demonstration of the QSH phase was realized in 2D quantum wells of HgTe/(Hg, Cd)Te at low temperatures.[1–4] Multi-probe resistance measurements in the quantum wells revealed hallmark transport conductance values, $\sim e^2/Nh$ (where e is the elemental electron charge, h is Planck's constant, and N is an integer), following the Landauer–Büttiker (LB) formalism that indicates dephasing of electron waves in metal electrodes placed on the 1D edge spin current path. Then, InAs/GaSb quantum wells have been a platform for the research of the QSH phase.[5,6]

On the other hand, atomically thin layers are expected as a major candidate for high-temperature 2D TIs. Indeed, prediction of the prototypical QSH insulator was in graphene, which is a carbon

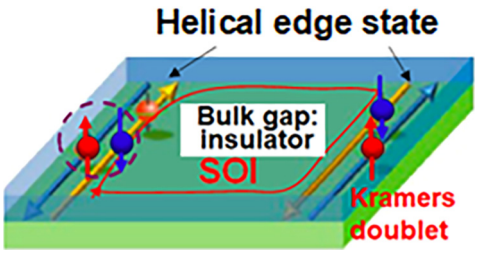

FIG. 1. Schematic view of helical edge states of 2D TI states.

monolayer.[9] However, graphene has extremely weak SOC because of the low mass of carbon atom and, hence, TI states are difficult to be detected. In order to overcome this problem, various theoretical works have reported how to induce SOC and introduce 2D TI states into graphene. Some experimental efforts have also been challenged. In Sec. II, this issue is reviewed introducing our latest experiments.[10–14,22–41]

Subsequently, monolayer (atomically thin) TMDC family (e.g., WTe_2, MoS_2) is becoming a strong candidate. Large internal electric fields caused by strong out-of-plane asymmetry of a TMDC layer induce a band inversion.[15–21] Moreover, heavy mass of TMDC atoms provides strong SOC. This SOC yields topological bulk gaps Δ in the band inversion. Furthermore, one of the crystal phases in TMDC family, the so-called 1T′ phase, possesses strain, resulting in the stable crystal structure. This strain also induces the band inversion and introduces huge, large Δ. Indeed, many works have observed such large Δ, which overcome even room-temperature energy, in the last few years.[16–18] Nevertheless, reports of high-temperature QSH phases are rare.[19–21] In Sec. III, this issue is reviewed basing on our experiments.

By combining superconductors (SCs) with helical edge spin states along the sample 1D edges of 2D TIs, one can explore various quantum phenomena and realize innovative application based on them. An interesting quantum phenomenon is the Majorana fermion (MF), which is an own anti-particle. The race for confirming MF and its application to topological quantum computation are highly active.[42–50] In Sec. IV, this MF issue is briefly discussed.

II. QSH PHASE IN GRAPHENE

Graphene played a key historical role in the development of TIs[7,8]—materials that demonstrate an electrically inert interior yet form exotic metals at their boundary. In 2005, Kane and Mele predicted that SOC of electrons turns graphene into a "QSH insulator" that hosts spin-filtered metallic edge states with inherent resilience from scattering.[9] These edge states were expected to activate tantalizing technological applications for dissipationless electronic and spintronic devices and fault-tolerant quantum computing.[10–12]

However, intrinsic SOC of graphene is far too weak to yield an observable QSH phase in practice. Various theoretical works have pursued this line of attack, e.g., by the introduction of foreign atoms or substrate engineering;[22–26] these methods were predicted to elevate the bulk bandgap for the QSH phase by several orders of magnitude compared to that in pure graphene. Implementation of these proposals was, however, so far proven challenging despite past efforts.[27–30]

On the other hand, numerous experimental trials have been made to enhance SOC and facilitate the observation of its QSH phase as follows; e.g., surface decoration by (1) small-mass adatoms[32,33] or (2) heavy nanoparticles[34–36] and (3) using heavy wires or substrates.[37–39] Nevertheless, they suffered from lack of appropriate experimental results with high reproducibility. One of the reasons for (1) and (2) is because precise control of the small-amount decoration (e.g., coverage ratio $\ll 10\%$) without giving damage or contamination was difficult. Moreover, large amount decoration (e.g., $\gg 10\%$) leads to various parasitic phenomena (e.g., spin absorption,[39,40] phase interference of electron spin waves or dephasing,[32] and inter-valley scattering) and obstructs emergence of pure SOC. Therefore, the small-amount and damageless decoration of graphene with nanoparticles is indispensable.

When these problems would be resolved, heavy adatom (nanoparticle) decoration theoretically leads to the introduction of SOCs into graphene. It preserves the sp^2 bond character (i.e., Dirac states) of graphene, while mediating diverse SOCs through electron tunneling onto and off the adatom *p,d,f*-orbitals, which depends on the position of the adatoms on the carbon hexagonal lattice of graphene. Many theoretical literature studies exist for this respect.

For example, SOC energy (E_{SO}) ~ 40 meV for a concentration of ~0.1 lead (Pb) adatom/carbon of graphene was theoretically predicted with a dependence of adatom density and position {e.g., hollow position [see Fig. 2(a)] or just above carbon atom}.[41] It was calculated that the latter position leads to the introduction of only Rashba-type SOC caused by the destruction of the out-of-plane symmetry of the graphene plane. On the contrary, both Rashba-type and intrinsic SOC can be introduced for the former case (i.e., hollow position). Even $E_{SO} > 200$ meV with a robust 2D TI state was predicted for $5d_{xz,\ yz}$-adatom [e.g., osmium (Os)] decorated graphene with coverage as small as 1% (on hollow position) [Figs. 2(a)–2(c)].[23] That was attributed to the hybridization of the partially filled *d*-orbital SOC impurity bands with the Dirac state of graphene [Figs. 2(d) and 2(e)]. Random and small-amount decoration (coverage $\ll 10\%$) can even stabilize topological phases.[24] Moreover, decoration of graphene by extremely small-amount nanoparticles can maintain ballistic electron transport, resulting in room-temperature detection of spin current. These features are beneficial. The first experimental evidence for the formation of the QSH phase in a graphene decorated with heavy nanoparticles has been confirmed experimentally as follows.

Graphene was decorated with dilute, randomly positioned Bi_2Te_3 nanoparticles at very small coverage (~3%), using nanoneedle methods in the experiments.[13,14] The strong chemical coupling between graphene Dirac stets and *d,f*-orbitals of Bi_2Te_3 nanoparticles was confirmed by x-ray photoelectron spectra (XPS). Although the XPS peak heights were small, the authors found that only the nanoparticle deposition via the nanoneedle method yields the small peaks because acetone droplets including nanoparticles were dropped on the graphene surface from the top end of nanoneedle, resulting in the introduction of very small amounts of damages or defects to the graphene surface.[14]

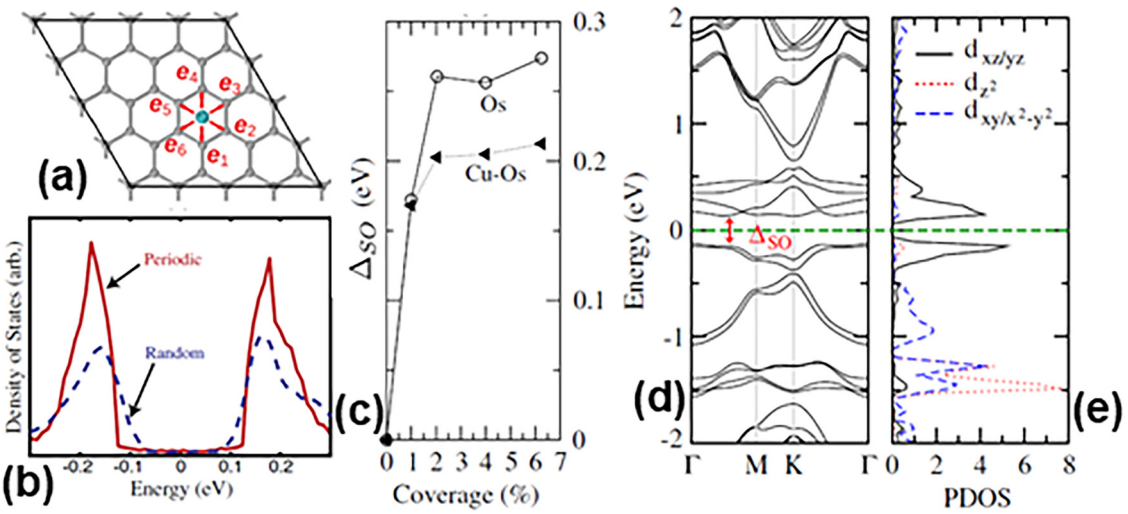

FIG. 2. (a) Schematic view of the hollow position for adatom placed on the center of carbon hexagonal lattice of graphene. (b) Topological bulk gap $\triangle_{so}$ as large as 200 meV, calculated for 1%-Os atom-decorated graphene at the hollow position. (c) Its coverage ratio dependence, including Cu–Os adatom cases, and (d) and (e) band structures for (b). Adapted and reproduced with permission from Hu *et al.*, Phys. Rev. Lett. **109**, 266801 (2012). Copyright 2012 The American Physics Society.

Non-local resistance measurements on six or four-probe pattern graphene with this nanoparticle coverage [insets of Figs. 3(a) and 3(b)] using back-gate voltages (V_{bg}) revealed quantitative agreement with the response expected from dissipationless edge-state conduction in a QSH phase, when the Fermi level (E_F) was tuned to Dirac points, i.e., confirmation of hallmark transport resistance values, quantum of resistance (R_Q) = $\sim e^2/2\,h$ [Fig. 3(a)] and $e^2/4\,h$ [Fig. 3(b)], following the LB formalism. These are in quantitatively good agreement with those for the QSH phase observed in HgTe/(Hg, Cd)Te quantum wells.[2]

The heavy nanoparticles carry giant SOC via tunneling current and can, thus, significantly modify graphene's Dirac states even at very low coverages; they can also be inserted into the graphene lattice in a minimally invasive way. As above-explained for heavy adatom/graphene systems, topological bulk gaps open due to the hybridization between the graphene's π states (the Dirac state) and the spin–orbit-split d_{xz} and d_{yz} Os atom orbitals in the case of Os adatom.[23] The Dirac state of graphene is rather delocalized and, thus, it can highly mediate interactions among Os adatoms over a large range even under small coverages. Figures 3(a) and 3(b) qualitatively coincide with this case. The perpendicular magnetic-field ($B_\perp$) dependence of the observed resistance peaks supported this.[14]

The temperature dependence of the resistance peaks clarified that the QSH phase can survive up to 25 K [Fig. 3(c)]. Scanning tunneling spectroscopy (STS) also suggested the presence of the maximum $\Delta \sim 20$ meV and its vanishing at the sample edges [Fig. 3(d)], supporting the presence of the 2D TI states. This experimental confirmation re-established graphene as an experimentally promising QSH medium and spotlighted many avenues of future exploration. However, the operating temperature for the QSH phase was still low, and the Δ values were small. Control of the nanoparticle decoration by the nanoneedle method is also not easy.

III. QSH PHASE IN THE 2D TMDC FAMILY

On the other hand, 2D TI states in various atomically thin 2D layers are recently attracting significant attention as candidates for the QSH phase with a huge large Δ, actually larger than room temperature (RT). They were theoretically predicted in Ref. 15, first, in the 1T′ phase of monolayer TMDC family.[15] After then, several experimental reports confirmed them by angle-resolved photoemission spectroscopy (ARPES) and STS, e.g., WSe_2 and WTe_2 [Figs. 4(a) and 4(b)], formed on bi-layer graphene/SiC with $\Delta \sim 100$–129 meV.[16] Other monolayers also confirmed large Δ, e.g., bismuthene (a bismuth monolayer) on SiC with $\Delta \sim 0.8$ eV,[17] and the layered mineral jacutingaite (Pt_2HgSe_3) with $\Delta \sim 110$ meV.[18]

The 1T′ phase of the monolayer TMDC family is particularly amenable to experimental scrutiny. In fact, large Δ have been detected in STS or ARPES at low temperatures. However, almost no reports of the QSH phase at high temperatures [e.g., by observing the R_Q/N ($=h/Ne^2$) like the cases for semiconductor quantum wells and graphene as introduced in Sec. II] existed. Only one work reported the 100 kelvin (K)-QSH phase in monolayer WTe_2 with a extremely short channel ($\ll\sim$100 nm) (Fig. 5).[19] In the report, a double-gate structure was employed. Whole gate tuned E_F to an energy far from Kramers point over the sample entire surface, resulting in the disappearance of 2D TI states and the introduction of the large metallic currents that suppress the large contact resistance between the metal electrode and WTe_2. In contrast, local gate tuned E_F to the Kramers point only in a very short channel between two electrodes, yielding 2D TI states and QSH phase up to 100 K (Fig. 5), which were obtained by low contact resistance.

For the lack of experimental evidence of the QSH phase at high temperature, the following origins are considered: (1) poor uniformity of Δ over the large sample area due to disorder induced by the substrate (doping or potential fluctuations), (2) influence of

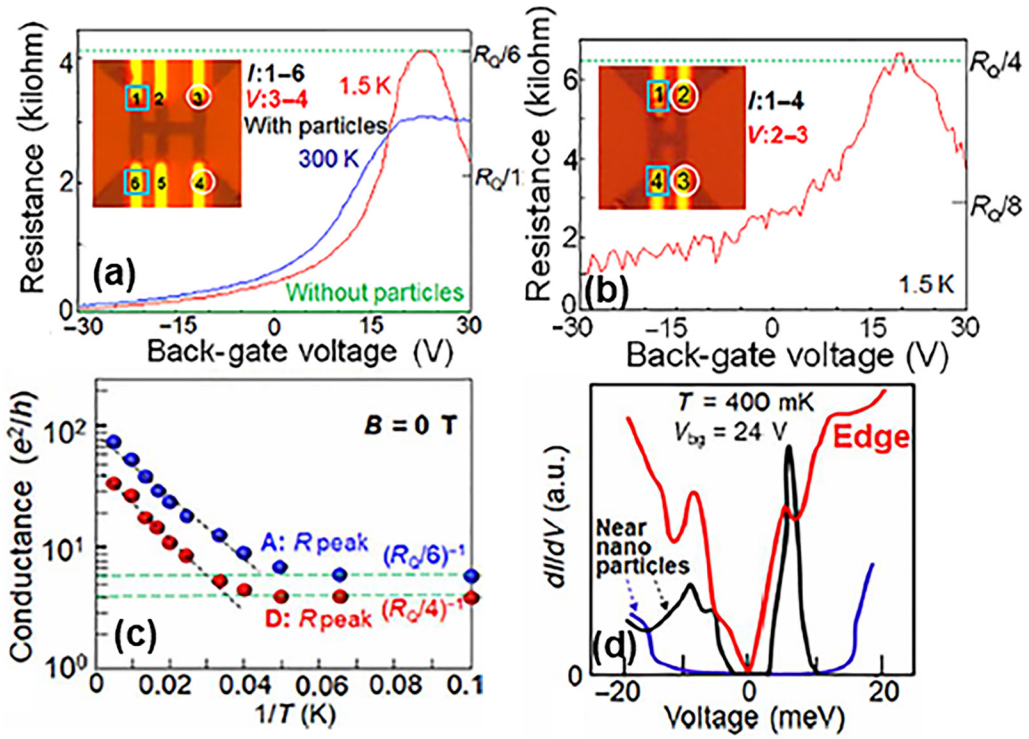

FIG. 3. Four-probe resistances (R) vs back-gate voltage (V_{bg}) measured on the graphenes formed into (a) six or (b) four-probe patterns (insets of a and b) and covered in Bi_2Te_3 nanoparticles at ∼3% coverage ratio. Current flows between contacts indicated by squares in insets, and R is measured across circled contacts; no contact Rs are subtracted. In (a), the green line corresponds to undecorated graphene. The green dashed line in each panel represents R_Q-based value predicted for helical edge transport. (c) Zero-B temperature dependence of conductance (in the Alenius plot format) corresponding to the inverse of the R peak values shown in Figs. 1(a) and 1(b); the dashed lines serve as a guide to the eye. (d) STS spectra for a sample around V_{bg} for the R peak, recorded at bulk locations near two different nanoparticles (black and blue curves) and at an edge point (red curve). Adapted from Hatsuda *et al.*, Sci. Adv. **4**, eaau6915 (2019). Copyright 2019 Author(s), licensed under a Creative Commons Attribution (CC BY) license.

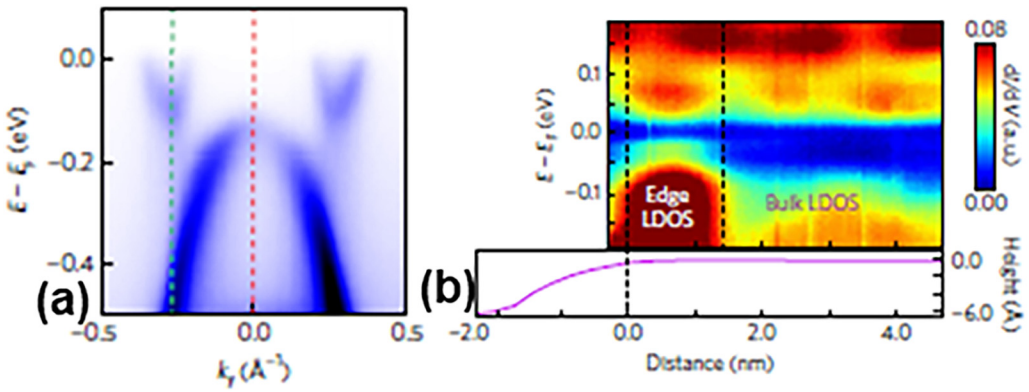

FIG. 4. (a) and (b) Large topological bulk gaps observed in angle-resolved photoemission spectroscopy (ARPES) for monolayer WSe_2 (a) and WTe_2 (b) formed on bi-layer graphene/SiC. (c) STS spectra of (a) on bulk and edge. Adapted and reproduced with permission from Tang *et al.*, Nat. Phys. **13**, 683 (2017). Copyright 2017 Springer Nature.

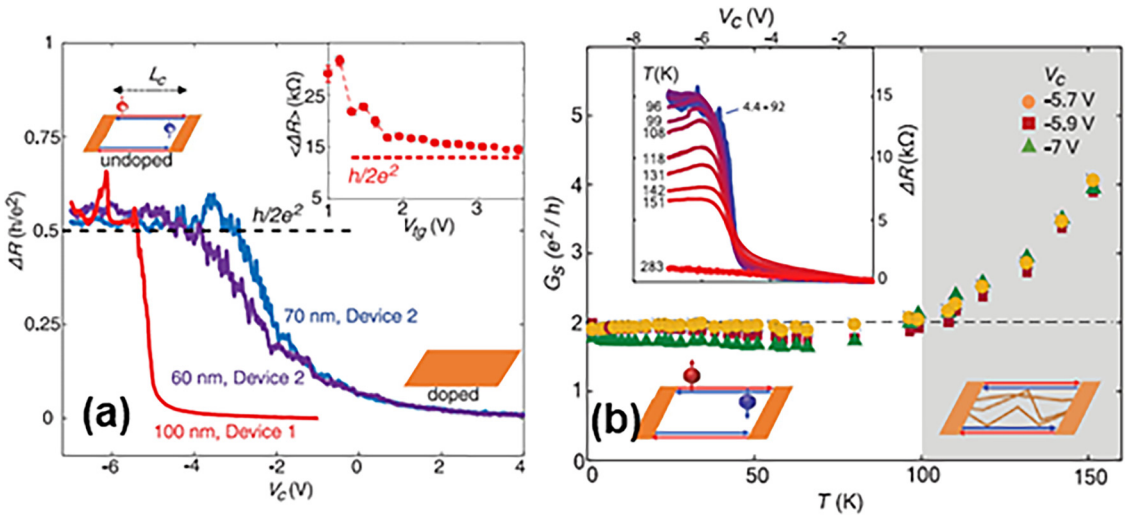

FIG. 5. (a) Quantum-spin-Hall phase observed in monolayer WTe_2 with dual gate structure. V_c is the local gate voltage that was applied between two-probe electrodes with very short channel length (i.e., ≪100 nm). (b) Its temperature dependence. Adapted and reproduced with permission from Wu *et al.*, Science **359**, 76 (2018). Copyright 2018 The American Association for the Advancement of Science.

oxidation (air exposure of samples), (3) influence of conducting substrates, which can short-circuit the edge states, and/or (4) noisy spectra of STS measured at high temperature. Regarding (1) and (2), the observation of a Δ by STS and ARPES gives only partial information. Even if the measured Δ are large, thermally activated charge carriers can overcome small values of Δ found at some regions of a large sample area. Thus, helical edge states can be disrupted, particularly at high temperatures. The 100K-QSH phase observed only in a noticeably short channel in the above-mentioned WTe_2 strongly supports this interpretation. Problem (3) can be minimized by using non-conductive substrates (e.g., *h*BN, SiO_2).

Problems (1) and (2) were resolved by a specific method, in which the 1T′–TI phase was patterned on 2H semiconducting-phase few-layer MoS_2 by laser-beam irradiation.[20,21] In-plane heat yielded by the laser irradiation rapidly and uniformly decays over large area of the TMDC layer surface, resulting in an increase in temperature up to ∼300 °C and causing a transition from the 2H to the 1T′–TI phases. Excess heat accumulation resulted in burning of the surface-side layers, leading to thinning layers and semitransparent color [Fig. 6(a)].

TMDC layers have various type phases; e.g., 2H semiconducting, 1T, and 1T′ phases [Fig. 6(b)]. Electron beam irradiation to the 2H phase causes a transition to the 1T phase, while it is metastable. In contrast, the 1T′ phase is more thermally and chemically stable, owing to the introduction of strain by decreasing the distance between two S atoms along the *z* direction (i.e., along out-of-plane) [Fig. 6(b)], which enables applications with long-term reliability. 1T′-phase TMDCs have been formed by various methods (e.g., laser-beam irradiation, substrate heating, and chemical vapor deposition on bi-layer graphene) and deployed in numerous applications (e.g., ohmic metallic junction between a metal electrode and 2H-MoS_2, supercapacitor electrodes, and the present TIs). Large internal electric fields caused by breaking of the out-of-plane (the *z* direction) symmetry in TMDCs yields a band inversion, and then, strong SOC due to the large mass opens topological Δ on this band inversion. The strain of the 1T′ phase also induces the band inversion, leading to the larger Δ.

As the initial laser-irradiation experiments, the formation of many 1T′-layers and an excessive damage done by the high-power laser beam (e.g., ∼17 mW) and long irradiation time (e.g., over ∼30 s) led to a 1T′ phase with sizable Δ ∼ 35 meV over a large area (∼2 μm), which showed traces of the QSH phase up to ∼40 K.[20] However, the laser-beam irradiation conditions to clearly obtain one quantized resistance plateau (peak) due to the QSH phase were not realized.

In their second experiments, the power and the irradiation time were improved with a power as low as 4.6 mW and irradiation

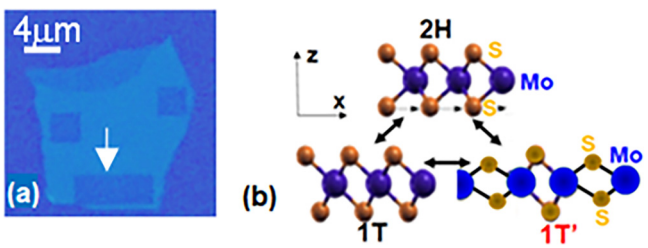

FIG. 6. (a) Optical microscope image of a MoS_2 flake. The semitransparent rectangle parts are the low-power laser-beam irradiated regions corresponding to 2D topological phase. The region shown by an arrow is used for the measurements for Figs. 7(a) and 7(b). (b) Schematic images of the crystal structure for 2H, 1T, and 1T′ phases of the TMDC family.

time of 20 s for each point and applied to thinner MoS_2 layers (~4 layers), which have been previously mechanically exfoliated from the bulk material and transferred onto a SiO_2/Si substrate.[21] This allowed us to clearly observe the RT-QSH phase arising from a protected topologically non-trivial mono(or bi)-layer embedded in the few-layer 1T′-MoS_2. Damages to the 1T′-phase crystal were suppressed by the lower laser power and its shorter irradiation times, particularly for the inner layers, which are protected by the top surface and bottom layers. These are likely to present a uniform high-crystal quality. Despite the low power employed, all layers of the 2H phase were changed into ~4 layers in the 1T′ phase.

RT resistance (R) measurements are shown in Figs. 7(a) and 7(b) as a function of V_{bg}.[21] Peaks or plateau-like features with values ~$R_Q/2$ appear in the two-probe measurements [Fig. 7(a)], which is consistent with the report in a short-channel monolayer of WTe_2.[19] This result was also a notable improvement upon the above-mentioned high-power laser-irradiation results, where, despite being promising, a single clear plateau was hardly obtained.[20] The slight deviation of the RT R peak values from theory ~$R_Q/2$ for the 0.5 μm-channel [Fig. 7(a)] and also those for the longest channel length (2 μm) were attributed to the thermally activated bulk charge carriers in some 1T′ topological parts with the smaller Δ and the defective edges (e.g., local charge puddles),[5,14,30,31] respectively.

A four-probe measurement reconfirmed this result [Fig. 7(b)], where a well-developed plateau with a value of $R_Q/4$ appears. The $R_Q/4$ value becomes even more well-defined at T = 1.5 K. This value was reported in the four-probe measurement on HgTe/(Hg, Cd)Te quantum wells,[2,3] Bi_2Te_3-nanoparticle decorated graphene (Sec. II), and in the above-mentioned high-power laser-irradiated thin 1T′ MoS_2. A straightforward calculation based on the LB formalism confirmed the measured value for this contact geometry.[21]

$B_\perp$-dependent measurements are shown in Fig. 7(c). As $B_\perp$ increases, the conductance G, corresponding to the inverse of $R_Q/2$ [red symbols; Figs. 7(a)] and $R_Q/4$ [blue symbols; Fig. 7(b)], exponentially decreases. G values (black symbols) corresponding to the inverse of R away from the peak or plateau remain almost unchanged. These results were in good agreement with those observed in WTe_2[19] and in Bi_2Te_3 decorated graphene (Sec. II), and further supported that the R peak (plateau) can be attributed to helical edge states. Only when E_F was set to the Kramers degeneracy point at $B_\perp = 0$, R can reflect the time-reversal symmetry breaking and gap opening caused by the applied $B_\perp$ (see insets), resulting in the observed exponential decrease in G.

Figure 7(d) demonstrates examples of low-temperature STS spectra taken on laser-irradiated 1T′ regions. For $V_{bg} \sim 35$ V, approximately corresponding to the Kramers degeneracy point (see schematic views in the insets), STS gaps of $\Delta \sim 60$–70 meV, which are larger than RT, are measured in two bulk points (blue and green curves), while the gap closes near an edge (red solid curve). The Δ values were also larger than 45-meV, as reported in 1T′-WTe_2.[19] Moreover, when V_{bg} was set away from the Kramers degeneracy point ($V_{bg} \sim 10$ V; red dotted curve) at the edge position (refer insets), dI/dV transformed into that expected for just the metallic behavior of the 1T′ phase.

This laser-derived 1T′ phase made the observation of the RT-QSH phase with high stability possible, which was maintained at least for 10 days in air. The laser-beam irradiation method brought several advantages into the field of atomically thin QSH crystals and also opened the possibility for RT applications of these topological phases. In particular, the on-demand laser-beam patterning of the topological phases on thin semiconducting MoS_2 regions facilitates the design of topological spintronic devices with zero-emission energy. Combining this with high-temperature superconductors could open the door to Majorana fermion based topological devices and circuits for high-temperature operation. The possibility is briefly demonstrated in Sec. IV.

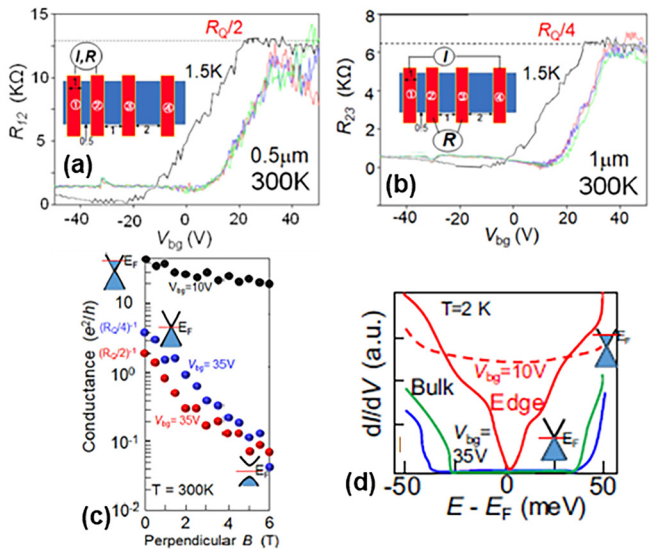

FIG. 7. (a) Two- and (b) four-probe R measurements as a function of V_{bg}. The low contact R is subtracted. Different colors of the three curves represent different measurements over three times. Dotted lines correspond to $R_Q/2$ and $R_Q/4$. Black curves are the results measured at 1.5 K. Insets: Schematic views of the electrode probe arrangement (red areas) on the 1T′ region with inter-probe (channel) distance expressed in μm. (c) Out-of-plane magnetic-field ($B_\perp$) dependence of conductance corresponding to the inverse of the R peak and plateau values in (a) and (b) (red and blue symbols) and to the inverse of a R value off peak (plateau) (black symbol). (d) STS spectra for the laser-irradiated 1T′ region. The two bulk signals (blue and green curves) were measured near the center of the 1T′ region, and the edge signals (red solid and dotted curves) were measured near the boundary of the 1T′/2H phases. V_{bg} was set to +35 V (corresponding to the R peak) and +10 V (to off R peak) for the three solid and the dotted curves, respectively. Insets: Schematic views of band diagrams near or away from Kramers degeneracy point with E_F. Adapted from Katsuragawa *et al.*, Commun. Mater. **1**, 51 (2020). Copyright 2020 Author(s), licensed under a Creative Commons Attribution (CC BY) license.

IV. MAJORANA ZERO-BIAS MODES IN A HYBRID SYSTEM FOR SC/HELICAL EDGE SPIN STATES

In Sec. III, how to realize the QSH phases of 2D TIs on TMDC family were reviewed. By combining SC- or ferromagnetic-electrodes with helical edge spin states along the sample 1D edges of 2D TIs, one can explore various quantum phenomena and realize innovative applications based on them.

One of exciting quantum phenomena is MF. First, the appearance of MF was predicted at edges and cores of topological superconductors [Fig. 8(a)] and then at the end edges of interface between SC and 1D helical edge states of 2D TIs or 1D-TI states under weak in-plane magnetic fields ($B_{//}$) [Figs. 8(b) and 8(c)]. Recently, signatures of MF are experimentally researched in a hybrid system for SC/semiconductor nanowires with strong SOI under weak $B_{//}$ [Fig. 8(d) and 8(e)],[42–45] including a proximity-induced superconducting Coulomb island (Majorana island).[46–48] Most recently, it is reported even in Fe-atomic chains/SC(Pb) system[49] and Kitaev spin liquid ($RuCl_3$).[50]

Signatures of MF in a hybrid system for SC/semiconductor nanowires with strong SOI have been confirmed by many observations of Majorana zero-bias modes (MZBM) [Fig. 8(e)], which are quasiparticle excitations in condensed matter systems and have been proposed as building blocks of fault-tolerant quantum computers. They may exhibit non-Abelian particle statistics, in contrast to the usual statistics of fermions and bosons, enabling quantum operations to be performed by braiding isolated modes around one another. Quantum braiding operations are topologically protected insofar as these modes are pinned near zero energy with the departure from zero expected to be exponentially small as the modes become spatially separated.

In contrast, none reported on MZBM in a hybrid system of SC/helical edge spin states of 2D TIs because report of the helical edge spin states was rare before our finding as mentioned in Secs. II and III. The 1D edge spin path of a helical edge state coupled with SCs may be highly effective to yield MF and its braiding. In particular, the laser patterning method as introduced in Sec. III allows on-demand patterning of the helical edge spin paths and positioning of MFs by combining with SCs. An example of investigation, whether MZBM can be detected in a system of SC/helical edge spin states in the few-layer 1T′ MoS_2 explained in Sec. III is briefly mentioned as following.

Figure 9(a) shows an optical microscope image of the measured sample for a hybrid system of the Nb/laser-derived TI region in few-layer MoS_2. The 1T′ phase region on few-layer MoS_2 was formed by the same low-power laser-irradiation conditions as those mentioned in Sec. III. Two Nb electrodes with the spacing of 500 nm were placed on one edge line of the laser-derived 1T′ phase region, which should have QSH phase based on the experiments in Sec. III.

Figure 9(b) shows dI/dV (differential conductance) vs voltage feature on different $B_{//}$ values of Fig. 9(a)—sample at $V_{bg} = 35$ V and T = 100 mK. A large gap (~1 mV) on dI/dV is observed at $B_{//} = 0$, while it decreases as $B_{//}$ increases. Expansion of $V \sim 0$ in the low $B_{//}$ region of Fig. 9(b) is shown in Fig. 9(c). It reveals the appearance of a small zero-bias dI/dV peak with the width of ~30 μV at $B_{//} \sim 300$ mT, whereas the peak disappears at a higher $B_{//}$ region. As mentioned above, such a dI/dV peak has been understood as a MZBM in a hybrid system for SC/semiconductor nanowires with strong SOI. A MZBM appears within an Andreev gap, which originates from the reflection of Cooper pairs at the interface of SC/semiconductor junctions. The gap value with ~1 mV width observed in Fig. 9(b) is two-times larger than Andreev gaps

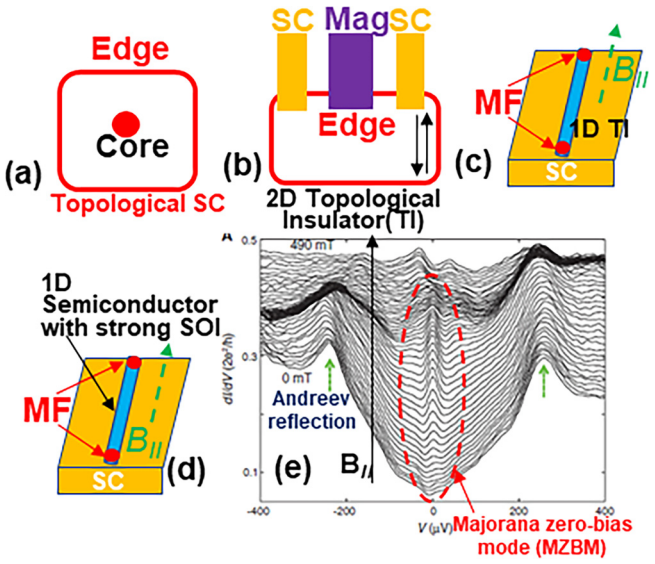

FIG. 8. (a)–(c) Schematic views for observing a Majorana fermion (MF). (a) Core and edges of topological superconductors (SCs), (b) hybrid of 1D helical edge states of 2D TIs and two SCs(S) under in-plane magnetic fields ($B_{//}$) caused by ferromagnetic electrode (M), and (c) hybrid of 1D-TI and SC. (d) Schematic view of hybrid system of SC and semiconductor nanowire with strong SOI under weak $B_{//}$. (e) MZBM on dI/dV vs V observed in (d) and (e); Adapted and reproduced with permission from Kato *et al.*, Science **336**, 1003 (2012). Copyright 2012 The American Association for the Advancement of Science.

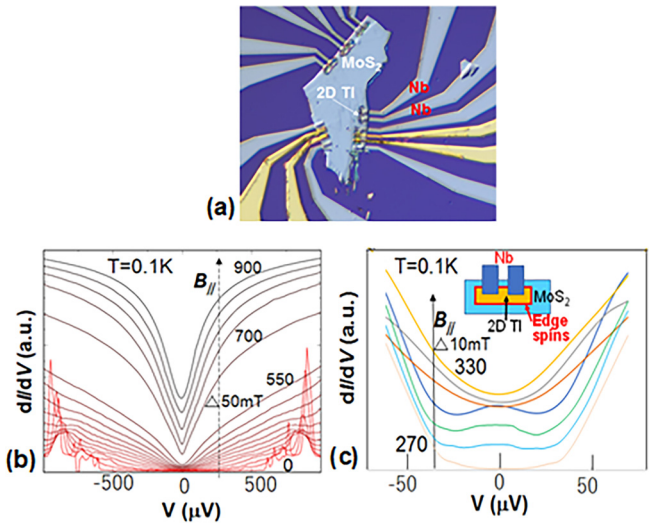

FIG. 9. (a) Optical microscope image of a MoS_2 flake with two Nb electrodes shown in white arrow as a measured part. (b) Two-probe differential conductance (dI/dV) measurements as a function of voltage on different in-plane magnetic fields ($B_{//}$) of (a)—sample at $V_{bg} = 35$ V. Each number for $B_{//}$ is in mT. (c) Expansion of $V \sim 0$ in the low $B_{//}$ region of (b). Inset: Schematic view of laser-derived 1T′ region with two Nb electrodes shown in (a).

~0.5 mV observed for Nb/semiconductor nanowires. In the present case, two Nb electrodes are placed on mainly the edge spin current path, and also the bulk gap part of the 2D TI region (<~0.5 μm) and the semiconducting MoS_2 region (<~0.5 μm), which locates at the flake edge and gives almost no contributes to current flow [see the inset of Fig. 9(b)]. Thus, the observed gap may be attributed to the interface between the purely 1D spin current path of the helical edge spins (i.e., ≪10 nm width) and Nb electrodes.

In contrast, the zero-bias peak width ~30 μV observed $B_{//} \sim 300$ mT is in approximately good agreement with the width of a MZBM ~ 10 μV observed at $B_{//} <$ ~400 mT for Nb/semiconductor (InSb) nanowires. This suggests the possible presence of MFs in our system. The shape of dI/dV vs V curves drastically changes at $B_{//} > 300$ mT (i.e., width of the dI/dV gap becomes larger) and the MZBM-like peak suddenly disappears. This may also be associated with $B_{//}$ dependence of the purely 1D spin current path. As mentioned in Sec. III, the QSH phase is highly sensitive to the Zeeman gap opening caused by $B_{\perp}$ and easily suppressed. If the applied $B_{//}$ may open such a gap at $B_{//} > 300$ mT, the helical edge spin currents are easily suppressed and a MZBM should disappear. Further investigation is needed to clarify this.

V. CONCLUSION

How to create 2D TIs with QSH phases were briefly reviewed for atomically thin or few-atom layers, graphene, and 2D TMDC family. Although graphene has less SOC, decoration with heavy nanoparticles (Bi_2Te_3) within only 3% coverage introduced the QSH phase. Few-atom-layer 1T′-phase MoS_2 created by low-power laser-beam irradiation realized the RT-QSH phase and allowed on-demand patterning of the QSH phases on few-layer semiconductors, resulting in feasible application in RT topological devices.

In contrast, various quantum phenomena, which provide the quantized conductance due to non-topological natures, exist. One of those in atomically thin layers is 1D edge conductance. Edge states can arise even in topologically trivial systems,[51–53] e.g., due to band bending[52] and edge defects[53] as observed in ordinary graphene near the Dirac point. Although quantized edge resistances were not reported in those graphene studies, it is indispensable to reconfirm whether the experimental results introduced here including the edge of laser-derived 1T′-phase regions are compatible with such a trivial scenario.

The possible presence of MZBM was also discussed by combining Nb electrodes to this QSH phase. Research of 2D TIs on atom-thin (or few) layer TMDCs and application of the topologically protected 1D edge spin currents of the QSH phases to innovative quantum devices must open a door to next-generation quantum architectures, such as MF-based topological quantum computation following non-Abelian particle statistics.

ACKNOWLEDGMENTS

The author thanks T. Nakamura, M. Onizaki, S. Katsumoto, T. Inoue, S. Maruyama, S. Murakami, T. Yamamoto, S. Tarucha, T. Ando, T. Enoki, J. J Palacios, A. MacDonald, R. Wu, J. Alicea, T.-C. Chiang, M. Dresselhaus, P. J.-Herrero, and P. Kim for their technical contributions, fruitful discussions, and encouragement.

DATA AVAILABILITY

The data that support the findings of this study are available within the article.

REFERENCES

[1]B. A. Bernevig, T. L. Hughes, and S.-C. Zhang, "Quantum spin Hall effect and topological phase transition in HgTe quantum wells," Science **314**, 1757 (2006).
[2]M. Konig, S. Wiedmann, C. Brüne, A. Roth, H. Buhmann, L. W. Molenkamp, X.-L. Qi, and S.-C. Zhang, "Quantum spin Hall insulator state in HgTe quantum wells," Science **318**, 766 (2007).
[3]A. Roth, C. Brüne, H. Buhmann, L. W. Molenkamp, J. Maciejko, X.-L. Qi, and S.-C. Zhang, "Nonlocal transport in the quantum spin Hall state," Science **325**, 294 (2009).
[4]C. Brüne, A. Roth, H. Buhmann, E. M. Hankiewicz, L. W. Molenkamp, J. Maciejko, X.-L. Qi, and S.-C. Zhang, "Spin polarization of the quantum spin Hall edge states," Nat. Phys. **8**, 485 (2012).
[5]L. J. Du, I. Knez, G. Sullivan, and R.-R. Du, "Robust helical edge transport in gated InAs/GaSb bilayers," Phys. Rev. Lett. **114**, 096802 (2015).
[6]C. Liu, T. L. Hughes, X.-L. Qi, K. Wang, and S.-C. Zhang, "Quantum spin Hall effect in inverted type-II semiconductors," Phys. Rev. Lett. **100**, 236601 (2008).
[7]M. Z. Hasan and C. L. Kane, "Colloquium: Topological insulators," Rev. Mod. Phys. **82**, 3045 (2010).
[8]X.-L. Qi and S.-C. Zhang, "Topological insulators and superconductors," Rev. Mod. Phys. **83**, 1057 (2011).
[9]C. L. Kane and E. J. Mele, "Quantum spin Hall effect in graphene," Phys. Rev. Lett. **95**, 226801 (2005).
[10]L. Fu and C. L. Kane, "Josephson current and noise at a superconductor/quantum-spin-Hall-insulator/superconductor junction," Phys. Rev. B **79**, 161408 (R) (2009).
[11]A. Y. Kitaev, "Fault-tolerant quantum computation by anyons," Ann. Phys. **303**, 2 (2003).
[12]C. Nayak, S. H. Simon, A. Stern, M. Freedman, and S. D. Sarma, "Non-Abelian anyons and topological quantum computation," Rev. Mod. Phys. **80**, 1083 (2008).
[13]T. Nanba, K. Tamura, K. Hatsuda, T. Nakamura, C. Ohata, S. Katsumoto, and J. Haruyama, "Spin–orbit interaction in Pt or Bi_2Te_3 nanoparticle-decorated graphene realized by a nanoneedle method," Appl. Phys. Lett. **113**, 053106 (2018).
[14]K. Hatsuda, H. Mine, T. Nakamura, J. Li, R. Wu, S. Katsumoto, and J. Haruyama, "Evidence for a quantum spin Hall phase in graphene decorated with Bi_2Te_3 nanoparticles," Sci. Adv. **4**, eaau6915 (2019).
[15]X. Qian, J. Liu, L. Fu, and J. Li, "Quantum spin Hall effect in two-dimensional transition metal dichalcogenides," Science **346**, 1344 (2014).
[16]P. Chen, W. W. Pai, Y.-H. Chan, W.-L. Sun, C.-Z. Xu, D.-S. Lin, M. Y. Chou, A.-V. Fedorov, and T.-C. Chiang, "Large quantum-spin-Hall gap in single-layer 1T′ WSe_2," Nat. Commun. **9**, 2003 (2018); S. Tang *et al.*, "Quantum spin Hall state in monolayer 1T′-WTe_2," Nat. Phys. **13**, 683 (2017).
[17]F. Reis R. Claessen *et al.*, "Bismuthene on a SiC substrate: A candidate for a high-temperature quantum spin Hall material," Science **357**, 287 (2017).
[18]K. Kandrai, G. Kukucska, P. Vancsó, J. Koltai, G. Baranka, Z. E. Horváth, Á. Hoffmann, A. Vymazalová, L. Tapasztó, and P. Nemes-Incze, "Signature of large-gap quantum spin Hall state in the layered mineral Jacutingaite," Nano Lett. **20**, 5207 (2020).
[19]S. Wu, V. Fatemi, Q. D. Gibson, K. Watanabe, T. Taniguchi, R. J. Cava, and P. Jarillo-Herrero, "Observation of the quantum spin Hall effect up to 100 kelvin in a monolayer crystal," Science **359**, 76 (2018).
[20]H. Mine, T. Nakamura, T. Inoue, S. Pakdel, S. Maruyama, S. Katsumoto, A. Fortunelli, J. J. Palacios, J. Haruyama *et al.*, "Laser-beam-patterned topological insulating states on thin semiconducting MoS_2," Phys. Rev. Lett. **123**, 146803 (2019).
[21]N. Katsuragawa, M. Nishizawa, T. Nakamura, T. Inoue, S. Pakdel, S. Maruyama, S. Katsumoto, J. J. Palacios, and J. Haruyama, "Room-temperature

quantum spin Hall phase in laser-patterned few-layer 1T′-MoS_2," Commun. Mater. **1**, 51 (2020).
[22]C. Weeks, J. Hu, J. Alicea, M. Franz, and R. Wu, "Engineering a robust quantum spin Hall state in graphene via adatom deposition," Phys. Rev. X **1**, 021001 (2011).
[23]J. Hu, J. Alicea, R. Wu, and M. Franz, "Giant topological insulator gap in graphene with 5d adatoms," Phys. Rev. Lett. **109**, 266801 (2012).
[24]H. Jiang, Z. Qiao, H. Liu, J. Shi, and Q. Niu, "Stabilizing topological phases in graphene via random adsorption," Phys. Rev. Lett. **109**, 116803 (2012).
[25]Y. Ren, Z. Qiao, and Q. Niu, "Topological phases in two-dimensional materials: A review," Rep. Prog. Phys. **79**, 066501 (2016).
[26]B. Yan, M. Jansen, and C. Felser, "A large-energy-gap oxide topological insulator based on the superconductor $BaBiO_3$," Nat. Phys. **9**, 709 (2013); D. Kong *et al.*, "Rapid surface oxidation as a source of surface degradation factor for Bi_2Se_3," ACS Nano **5**, 4698 (2011).
[27]Z. Jia, B. Yan, J. Niu, Q. Han, R. Zhu, D. Yu, and X. Wu, "Transport study of graphene adsorbed with indium adatoms," Phys. Rev. B **91**, 085411 (2015).
[28]U. Chandni, E. A. Henriksen, and J. P. Eisenstein, "Transport in indium-decorated graphene," Phys. Rev. B **91**, 245402 (2015).
[29]Y. Wang, S. Xiao, X. Cai, W. Bao, J. Reutt-Robey, and M. S. Fuhrer, "Electronic transport properties of Ir-decorated graphene," Sci. Rep. **5**, 15764 (2015).
[30]A. F. Young, J. D. Sanchez-Yamagishi, B. Hunt, S. H. Choi, K. Watanabe, T. Taniguchi, R. C. Ashoori, and P. Jarillo-Herrero, "Tunable symmetry breaking and helical edge transport in a graphene quantum spin Hall state," Nature **505**, 528 (2014).
[31]S. Essert and K. Richter, "Magnetotransport in disordered two-dimensional topological insulators: Signatures of charge puddles," 2D Mater. **2**, 024005 (2015).
[32]J. Balakrishnan, G. K. W. Koon, M. Jaiswal, A. H. Castro Neto, and B. Ozyilmaz, "Colossal enhancement of spin–orbit coupling in weakly hydrogenated graphene," Nat. Phys. **9**, 284 (2013).
[33]T. Kato, J. Kamijo, T. Nakamura, C. Ohata, S. Katsumoto, and J. Haruyama, "Spin phase protection in interference of electron spin waves in lightly hydrogenated graphene," RSC Adv. **6**, 67586 (2016).
[34]J. Balakrishnan, G. K. W. Koon, A. Avsar, Y. Ho, J. H. Lee, M. Jaiswal, S.-J. Baeck, J.-H. Ahn, A. Ferreira, M. A. Cazalilla, A. H. C. Neto, and B. Özyilmaz, "Giant spin Hall effect in graphene grown by chemical vapour deposition," Nat. Commun. **5**, 4748 (2014).
[35]D. Van Tuan, J. M. Marmolejo-Tejada, X. Waintal, B. K. Nikolić, S. O. Valenzuela, and S. Roche, "Spin Hall effect and origins of nonlocal resistance in adatom-decorated graphene," Phys. Rev. Lett. **117**, 176602 (2016).
[36]Y. Wang, X. Cai, J. Reutt-Robey, and M. S. Fuhrer, "Universal sequence of ground states validating the classification of frustration in antiferromagnetic rings with a single bond defect," Phys. Rev. B **92**, 161411(R) (2015).
[37]W. S. Torres, J. F. Sierra, L. A. Benitez, F. Bonell, M. V. Costache, and S. O. Valenzuela, "Spin precession and spin Hall effect in monolayer graphene/Pt nanostructures," 2D Mater. **4**, 041008 (2017).
[38]T. Kimura, Y. Otani, T. Sato, S. Takahashi, and S. Maekawa, "Room-temperature reversible spin Hall effect," Phys. Rev. Lett. **98**, 156601 (2007).
[39]L. Vila, T. Kimura, and Y. Otani, "Evolution of the spin Hall effect in Pt nanowires: Size and temperature effects," Phys. Rev. Lett. **99**, 226604 (2007).
[40]Y. Niimi, Y. Kawanishi, D. H. Wei, C. Deranlot, H. X. Yang, M. Chshiev, T. Valet, A. Fert, and Y. Otani, "Giant spin Hall effect induced by skew scattering from bismuth impurities inside thin film CuBi alloys," Phys. Rev. Lett. **109**, 156602 (2012).
[41]L. Brey, "Spin-orbit coupling in graphene induced by adatoms with outer-shell p orbitals," Phys. Rev. B **92**, 235444 (2015).
[42]L. Fu and C. L. Kane, "Superconducting proximity effect and Majorana fermions at the surface of a topological insulator," Phys. Rev. Lett. **100**, 096407 (2008).
[43]V. Mourik, K. Zuo, S. M. Frolov, S. R. Plissard, E. P. A. M. Bakkers, and L. P. Kouwenhoven, "Signatures of Majorana fermions in hybrid superconductor-semiconductor nanowire devices," Science **336**, 1003 (2012).
[44]L. P. Rokhinson, X. Liu, and J. K. Furdyna, "The fractional ac Josephson effect in a semiconductor–superconductor nanowire as a signature of Majorana particles," Nat. Phys. **8**, 795–799 (2012).
[45]O. Gul, L. P. Kouwenhoven *et al.*, "Ballistic Majorana nanowire devices," Nat. Nanotechnol. **13**, 192–197 (2018).
[46]S. M. Albrecht *et al.*, "Exponential protection of zero modes in Majorana islands," Nature **531**, 206–209 (2016).
[47]M. T. Deng *et al.*, "Majorana bound state in a coupled quantum-dot hybrid-nanowire system," Science **354**, 1557–1562 (2016).
[48]H. Zhang *et al.*, "Quantized Majorana conductance," Nature **556**, 74 (2018).
[49]S. Nadj-Perge *et al.*, "Observation of Majorana fermions in ferromagnetic atomic chains on a superconductor," Science **346**, 602–607 (2014).
[50]Y. Kasahara *et al.*, "Majorana quantization and half-integer thermal quantum Hall effect in a Kitaev spin liquid," Nature **599**, 227–231 (2018).
[51]F. Nichele *et al.*, "Edge transport in the trivial phase of InAs/GaSb," New J. Phys. **18**, 083005 (2016).
[52]M. T. Allen, O. Shtanko, I. C. Fulga, A. R. Akhmerov, K. Watanabe, T. Taniguchi, P. Jarillo-Herrero, L. S. Levitov, and A. Yacoby, "Spatially resolved edge currents and guided-wave electronic states in graphene," Nat. Phys. **12**, 128 (2016).
[53]M. J. Zhu *et al.*, "Edge currents shunt the insulating bulk in gapped graphene," Nat. Commun. **8**, 14552 (2017).